

Precision Spectroscopy of Polarized Molecules in an Ion Trap

H. Loh,^{1*} K. C. Cossel,¹ M. C. Grau,¹ K.-K. Ni,^{1†} E. R. Meyer,² J. L. Bohn,¹ J. Ye,^{1*} E. A. Cornell^{1*}

Polar molecules are desirable systems for quantum simulations and cold chemistry. Molecular ions are easily trapped, but a bias electric field applied to polarize them tends to accelerate them out of the trap. We present a general solution to this issue by rotating the bias field slowly enough for the molecular polarization axis to follow but rapidly enough for the ions to stay trapped. We demonstrate Ramsey spectroscopy between Stark-Zeeman sublevels in $^{180}\text{Hf}^{19}\text{F}^+$ with a coherence time of 100 milliseconds. Frequency shifts arising from well-controlled topological (Berry) phases are used to determine magnetic g factors. The rotating-bias-field technique may enable using trapped polar molecules for precision measurement and quantum information science, including the search for an electron electric dipole moment.

Quantum control of the rich internal structure of molecules may lead to advances in both fundamental and applied physics beyond those already gleaned from atoms (1). The same complex molecular structure makes it difficult to trap neutral molecules; in contrast, molecular ions can be easily trapped by time-dependent electric fields (2–9). However, the use of an ion trap has precluded taking advantage of the electric dipole moment of molecular ions, a vital ingredient of many experiments ranging from precision tests of fundamental physics (2, 6, 10) to quantum information (11).

The ability to polarize the molecules is, for example, a prerequisite for a search for the electron electric dipole moment (eEDM) with molecules (12): This search serves as a direct tabletop test of time-reversal violation (13) and as a probe of physics beyond the Standard Model (14). Trapped HfF^+ or ThF^+ molecular ions in the $^3\Delta_1$ state are excellent candidates for an eEDM search with several key advantages: small Ω -doublet splitting for a built-in rejection of many systematic errors (15–17), small magnetic moment for reduced magnetic field sensitivity (18), long coherence times for spectroscopy, and high inter-

nal electric fields for enhanced eEDM sensitivity (2, 18–20). To access the high internal field, the molecules need to be polarized in the laboratory frame by an applied bias electric field; however, their position in the ion trap ensures that the time-averaged electric field is zero.

To address this issue, we apply a rotating bias electric field, realizing the proposal of (2). The frequency of rotation ω_{rot} is low enough for the molecular polarization axis to adiabatically follow the electric field but high enough for the ions to stay trapped.

At the heart of our experiment is a linear Paul trap with six radial confinement electrodes (Fig. 1, A and B). To form the rotating bias electric field \vec{E}_{rot} , we apply a set of sinusoidal voltages to the radial electrodes, such that the phases on successive electrodes are each advanced by 60° . \vec{E}_{rot} causes the molecular ions to rotate in a circular micromotion (Fig. 1B). Compared to all other forms of ion motion, including radiofrequency micromotion, the circular micromotion occurs on the fastest time scale. The fast time scale, com-

¹JILA, National Institute of Standards and Technology (NIST), and University of Colorado, and Department of Physics, University of Colorado, Boulder, CO 80309–0440, USA. ²Department of Physics, Kansas State University, Manhattan, KS 66506–2601, USA.

*Corresponding author. E-mail: loh@jilau1.colorado.edu (H.L.); ye@jila.colorado.edu (J.Y.); cornell@jila.colorado.edu (E.A.C.)

†Present address: Department of Chemistry and Chemical Biology, Harvard University, Cambridge, MA 02138, USA.

Fig. 1. Rotating-bias-field technique. (A) Three-dimensional view of a linear Paul trap (axial-confinement electrodes not shown). The colored radially confining electrodes carry an additional set of phase-shifted sinusoidal voltages to create a rotating bias field \vec{E}_{rot} . The pair of anti-Helmholtz coils creates a static magnetic-field gradient. (B) Top view of ion trap, with a depletion laser propagating between two radial electrodes. In one rotation cycle, the magnetic field (gray arrows) sampled by a molecular ion can be decomposed into a rotating component \vec{B}_{rot} and a time-invariant component \vec{B}_{static} . (C) Rotating-frame HfF^+ energy level diagram for the $^3\Delta_1$ ($v=0, J=1, F=3/2$) state in the presence of \vec{E}_{rot} and \vec{B}_{rot} . \vec{E}_{rot} splits the levels into four spectroscopically isolated Stark pairs. (D) Energies of sublevels within a single Stark pair. The rotation of the electric bias field couples the two sublevels, turning the linear Zeeman splitting (dashed lines) into an avoided crossing (solid lines) split by Δ at the point of zero B_{rot} . For a typical measurement, the Stark splitting, rotation rate, Zeeman splitting, and avoided-crossing mixing are given by 10 MHz, 250 kHz, 100 Hz, and 30 Hz, respectively.

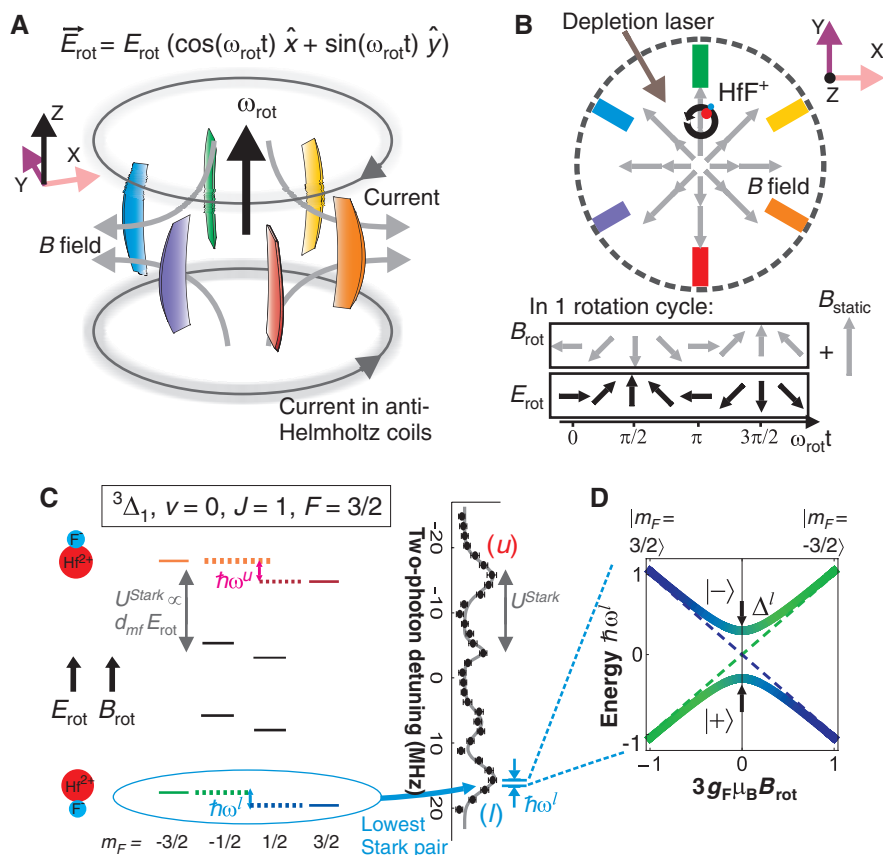
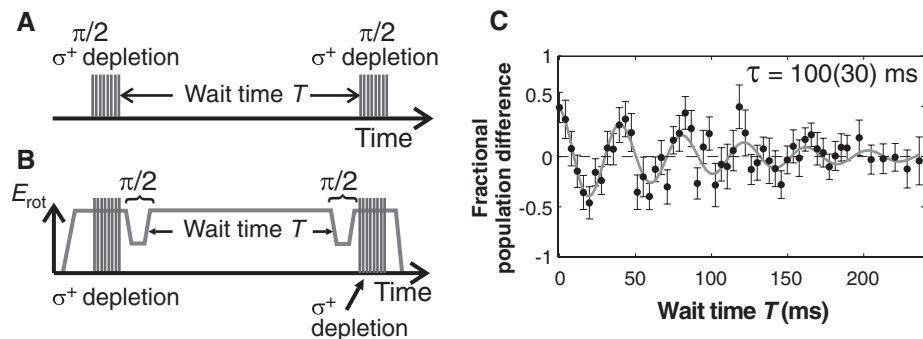
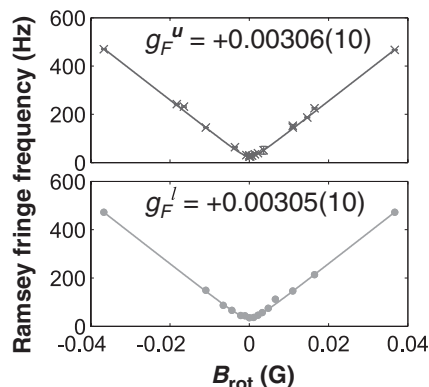


Fig. 2. Ramsey spectroscopy in rotating fields.

Ramsey sequences (A) for $B_{\text{rot}} = 0$, where the σ^+ -polarized depletion laser acts as both a polarizer and a $\pi/2$ pulse; (B) for high B_{rot} , where ramps in E_{rot} act as $\pi/2$ pulses. (C) Fractional difference of ions in $|m_F = 3/2\rangle$ versus that in $|m_F = -3/2\rangle$ as a function of the Ramsey wait time T , taken at $B_{\text{rot}} = 0$. The data are fit to a sinusoidal function with an exponential-decay time constant τ .


Fig. 3. Measurement of the avoided-crossing splitting.

Avoided crossing for $E_{\text{rot}} = 11.6$ V/cm, experimentally mapped out using Ramsey spectroscopy for the upper (crosses) and lower (dots) Stark pairs. The upper and lower pair magnetic g factors g_F that have been obtained from the fits (solid lines) are nearly identical and quite small.



binning with the spatial uniformity and large amplitude of E_{rot} , ensures that all the ions synchronously undergo the same circular micromotion. In this paper, the quantization axis is given by the instantaneous electric field.

For a precision measurement of the eEDM, it is advantageous to apply a magnetic field aligned along or against the bias electric field because the Zeeman interaction between the electron magnetic dipole moment and the magnetic field shifts the eEDM signal away from possible low-frequency noise sources. In our experiment, such a magnetic field can be implemented by combining a static magnetic-field gradient with the ions' circular micromotion (Fig. 1B). The magnetic field experienced by an ion over a rotation cycle can be decomposed into a spatially dependent but roughly time-invariant component $\mathbf{B}_{\text{static}}(\mathbf{R})$ and a time-varying, almost spatially independent component $\mathbf{B}_{\text{rot}}(t) = \mathbf{r}_{\text{rot}}(t) \partial B_p / \partial \rho$, where $\mathbf{r}_{\text{rot}}(t)$ is the circular micromotion and B_p is the radial component of the magnetic field. $\mathbf{B}_{\text{static}}$ can be safely neglected because the rotating bias electric field results in sensitivity to only \mathbf{B}_{rot} (2).

In the presence of a bias electric field and a coparallel magnetic field, the rotating-frame energy levels of the metastable $^3\Delta_1$ ($v = 0, J = 1, F = 3/2$) state of HfF^+ are split, where v is the vibrational quantum number, J is the rotational quantum number, and F is the hyperfine quantum number (Fig. 1C). The interaction between the molecules' electric dipole moment and the bias field gives rise to four pairs of Stark-split levels. The Stark spectrum in Fig. 1C is recorded by

performing two-photon Raman transfer to populate ions in the desired $^3\Delta_1$ state from the ground $^1\Sigma^+$ state via an intermediate $^3\Pi_{0+}$ state. A particular Stark level-pair can thus be isolated by tuning the Raman transfer laser frequencies to the appropriate two-photon resonance.

For the eEDM measurement, we focus on either the uppermost (u) or lowermost (l) Stark pairs. In the absence of B_{rot} , the coupling from the electric field rotation results in an avoided crossing of the two eigenstates ($|+\rangle$ and $|-\rangle$) separated by the energy splitting Δ . The eigenstates are equal superpositions of the spin projections, i.e. $|\pm\rangle_{B_{\text{rot}}=0} = (|m_F = 3/2\rangle \pm |m_F = -3/2\rangle) / \sqrt{2}$, where m_F is the spin-projection quantum number. As the Zeeman energy increases relative to Δ , the eigenstates of the Hamiltonian evolve from different superpositions of $|m_F = \pm 3/2\rangle$ to pure spin states (Fig. 1D). For sufficiently large magnetic fields, the energy eigenstates at high B_{rot} are $|\pm\rangle = |m_F = \pm 3/2\rangle$ and their energies asymptote toward a linear Zeeman shift. In the presence of the avoided crossing, the rotating magnetic field is not merely an advantage for precision measurement; it is a necessity for experiments aiming to manipulate states of distinct m_F .

To probe the physics of the rotating-frame Hamiltonian within a single Stark pair, we perform Ramsey spectroscopy on the individual sub-levels as a function of the rotating magnetic field. The Ramsey sequence always begins with populating ions in a single Stark pair and then optically pumping away ions in the $|m_F = -3/2\rangle$ state using a σ^+ -polarized depletion laser. For small B_{rot}

(i.e., small Zeeman splitting compared to Δ), the depletion process acts like a $\pi/2$ pulse, leaving the ions in a superposition of the eigenstates $|\pm\rangle$ (Fig. 2A). At high B_{rot} , the $\pi/2$ pulse is instead executed by fast ramps of the rotating electric field to and from a lower magnitude (21). The full Ramsey sequence (Fig. 2B) is the same as that used for an eEDM measurement.

The number of ions in either one of the two $|m_F\rangle$ states after the second $\pi/2$ pulse is determined by photodissociating the remaining ions in the $^3\Delta_1, J = 1$ state, and counting the dissociated ions via a mass-resolved ejection sequence. The fractional population difference between the two $|m_F\rangle$ states oscillates as a function of the wait time T between the two $\pi/2$ pulses at a frequency that is the avoided-crossing splitting (Fig. 2C). The decay time constant of the Ramsey fringe shows the ions maintaining coherence over a long period of 100(30) ms. The correspondingly high spectral resolution on the eEDM transition reduces vulnerability to potential systematic effects. The coherence time can potentially reach beyond 1 s, which is set by the $^3\Delta_1$ spontaneous-decay lifetime. The present limit most likely comes from ion-ion interactions.

Figure 3 shows the full avoided-crossing splittings for the upper and lower Stark pairs as a function of B_{rot} with a rotating bias field of 11.6 V/cm. A fit to the data yields the magnitude of the magnetic g factor, which is spectroscopically relevant for the eEDM experiment. We measured $g_F \equiv (g_F^u + g_F^l) / 2 = +0.00306(10)$ and the difference in g factors to be $\delta g_F = g_F^u - g_F^l = 0.00001(2)$. As expected, $g_F \ll 1$ due to the cancellation of orbital and spin angular momenta in the $^3\Delta_1$ state (2). Further, the magnetic g factor is similar for both the upper and lower Stark manifolds, which is advantageous for suppressing systematic errors in an eEDM experiment. A nonzero electron EDM would lead to a horizontal offset of the upper and lower curves in Fig. 3 from each other. The data shown represent our first eEDM measurement and already constrain its magnitude to be less than 1.5×10^{-25} e-cm. A dedicated eEDM effort may lead to a statistical uncertainty of 1×10^{-28} e-cm in a day (21).

A Ramsey-spectroscopy measurement of the electron EDM will determine its sign relative to the sign of the molecule's magnetic g factor. Our

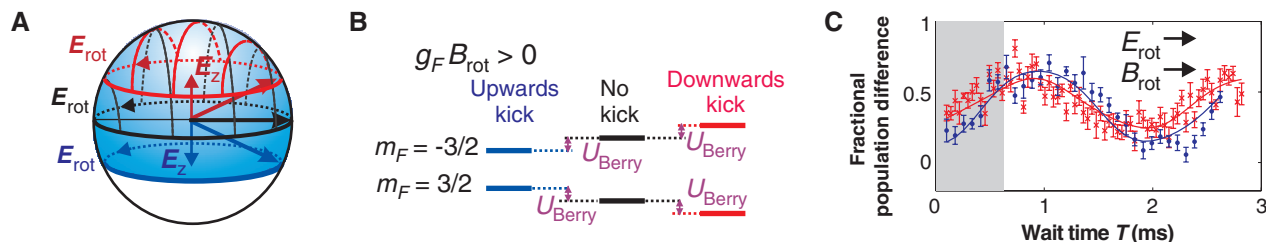


Fig. 4. Determination of the sign of the magnetic g factor using Berry phase. (A) Ions rotating in the $z = 0$ plane subtend a solid angle of 2π (black hatched hemisphere). As the ions are kicked above (below) the plane of rotation, they sample a force-restoring axial electric field E_z . The quantization axis thus tilts away from the plane of rotation, subtending a larger (smaller) solid angle indicated by the blue shaded (red hatched) region. (B) For $g_F B_{\text{rot}} > 0$, the additional Berry energy U_{Berry} from the axial kicks causes the $|m_F = \pm 3/2\rangle$

levels to move closer together or farther apart in energy. (C) Ramsey fringes recorded for $B_{\text{rot}} > 0$ (i.e., B_{rot} in phase with E_{rot}), where the ions have been kicked above (blue dots) or below (red crosses) the plane of rotation. The relative phase shifts mean $g_F > 0$. The gray shaded region corresponds to half an axial trap oscillation, which is the time over which the ions are exclusively in either the $z > 0$ or $z < 0$ region. The solid lines are fits to the data, incorporating the frequency chirp expected as the ions oscillate axially.

tool for determining the sign of g_F is the Berry phase (22).

The Berry phase is a dynamical phase shift imprinted on a quantum mechanical state due to the Hamiltonian having explicit time dependence. Under the influence of a rotating bias field, the ions can accumulate a finite Berry phase if the quantization axis is tilted away from the plane of rotation (23). In our technique, the resultant Berry phase is much better controlled across the ion cloud compared with that for a trapped sample of neutrals (24, 25).

To demonstrate this control, we explicitly incorporate its spectroscopic effect by giving the ions an impulse axial kick before performing the Ramsey sequence in a finite positive rotating magnetic field. The ions subsequently oscillate at the axial trap frequency. The Ramsey sequence is completed while the ions have only gone through half an axial oscillation, such that they are only present in either the $z > 0$ ($z < 0$) region for an upward (downward) kick. The downward-pointing (upward-pointing) trap field causes the quantization axis to tilt out of the plane of rotation, such that the solid angle Ω_{SA} subtended by the quantization axis is larger (smaller) than that without the kick (Fig. 4A). The resulting Berry phase ϕ_{Berry} manifests as a Berry energy $U_{\text{Berry}} = -\frac{\hbar\dot{\phi}_{\text{Berry}}}{(2\pi)/\omega_{\text{rot}}} = \hbar m_F \frac{\Omega_{\text{SA}}}{2\pi} \Omega_{\text{SA}}$ over one rotation cycle. For $g_F B_{\text{rot}} > 0$, the $m_F = 3/2$ level lies below the $m_F = -3/2$ level, so U_{Berry} causes the two m_F levels to move closer (split further apart) for an upward (downward) kick (see Fig. 4B). For a smaller (larger) energy splitting, the Ramsey fringe frequency is slower (faster), which looks like the Ramsey fringe has accumulated a positive (negative) initial phase shift. The two Ramsey fringes separately recorded with the ions kicked upward (dots) and downward (crosses) from the plane of rotation have a positive and negative phase shift, respectively (shaded region of Fig. 4C), which means that $g_F B_{\text{rot}} > 0$. Because $B_{\text{rot}} > 0$, we determine the magnetic g factor to be positive.

We have demonstrated coherent spectroscopy with molecular ions that are simultaneously polarized and trapped in a linear Paul trap with a

rotating bias field. The rotating bias field and corotating magnetic field open up access to the manipulation of Stark-Zeeman sublevels within a hyperfine-rovibronic state. The long coherence time of a qubit encoded by Stark-Zeeman states, whose relative energies are much more stable (compared with rotational or even hyperfine levels) against Stark-shift-induced decoherence mechanisms, is useful for quantum information processing (11). For quantum simulation experiments, the direct ability to manipulate dipolar interactions with molecular ions potentially eliminates the need for using optical spin-dependent forces to achieve spin-spin couplings, as is the case for trapped atomic ions (26–28). Further, the 10-Hz-level high-resolution spectroscopy is directly relevant to precision tests of ab initio theory (6), time variations in fundamental constants (29), and symmetry violations (30).

Note added in proof: We recently became aware of a new eEDM result from the ACME collaboration by Baron *et al.* (31).

References and Notes

- L. D. Carr, D. DeMille, R. V. Krems, J. Ye, *New J. Phys.* **11**, 055049 (2009).
- A. E. Leanhardt *et al.*, *J. Mol. Spectrosc.* **270**, 1–25 (2011).
- S. Willitsch, M. T. Bell, A. D. Gingell, T. P. Softley, *Phys. Chem. Chem. Phys.* **10**, 7200–7210 (2008).
- P. F. Staunum, K. Højbjerg, P. S. Skyt, A. K. Hansen, M. Drewsen, *Nat. Phys.* **6**, 271–274 (2010).
- J. H. V. Nguyen *et al.*, *New J. Phys.* **13**, 063023 (2011).
- U. Bressel *et al.*, *Phys. Rev. Lett.* **108**, 183003 (2012).
- S. Ding, D. Matsukevich, *New J. Phys.* **14**, 023028 (2012).
- J. E. Goeters *et al.*, *J. Phys. Chem. A* **117**, 9725–9731 (2013).
- W. G. Rellergert *et al.*, *Nature* **495**, 490–494 (2013).
- J. K. Thompson, S. Rainville, D. E. Pritchard, *Nature* **430**, 58–61 (2004).
- D. I. Schuster, L. S. Bishop, I. L. Chuang, D. DeMille, R. J. Schoelkopf, *Phys. Rev. A* **83**, 012311 (2011).
- J. J. Hudson *et al.*, *Nature* **473**, 493–496 (2011).
- I. B. Khriplovich, S. K. Lamoreaux, *CP Violation Without Strangeness: Electric Dipole Moments of*

Particles, Atoms and Molecules (Springer, Berlin, 1997).

- E. D. Commins, in *Advances in Atomic, Molecular and Optical Physics*, vol. 40, B. Bederson, H. Walther, Eds. (Academic Press, 1999), pp. 1–55.
- D. DeMille *et al.*, *Phys. Rev. A* **61**, 052507 (2000).
- S. Eckel, P. Hamilton, E. Kirilov, H. W. Smith, D. DeMille, *Phys. Rev. A* **87**, 052130 (2013).
- A. C. Vutha *et al.*, *J. Phys. B* **43**, 074007 (2010).
- E. R. Meyer, J. L. Bohn, M. P. Deskevich, *Phys. Rev. A* **73**, 062108 (2006).
- A. N. Petrov, N. S. Mosyagin, T. A. Isaev, A. V. Titov, *Phys. Rev. A* **76**, 030501 (2007).
- E. R. Meyer, J. L. Bohn, *Phys. Rev. A* **78**, 010502 (2008).
- Supplementary materials are available on Science Online.
- M. V. Berry, *Proc. R. Soc. Lond. A Math. Phys. Sci.* **392**, 45–57 (1984).
- E. R. Meyer, A. E. Leanhardt, E. A. Cornell, J. L. Bohn, *Phys. Rev. A* **80**, 062110 (2009).
- J. M. Pendlebury *et al.*, *Phys. Rev. A* **70**, 032102 (2004).
- M. Rupasinghe, N. E. Shafer-Ray, *Phys. Rev. A* **78**, 033427 (2008).
- D. Porras, J. I. Cirac, *Phys. Rev. Lett.* **92**, 207901 (2004).
- K. Kim *et al.*, *Phys. Rev. Lett.* **103**, 120502 (2009).
- J. W. Britton *et al.*, *Nature* **484**, 489–492 (2012).
- V. V. Flambaum, M. G. Kozlov, *Phys. Rev. Lett.* **99**, 150801 (2007).
- H. Müller, S. Herrmann, A. Saenz, A. Peters, C. Lammerzahl, *Phys. Rev. D Part. Fields Gravit. Cosmol.* **70**, 076004 (2004).
- J. Baron *et al.*, arXiv:1310.7534 (2013).

Acknowledgments: This work is supported by NIST, the Marsico Foundation, and NSF grant number 1125844. H. L. is partly funded by the Agency for Science, Technology and Research (Singapore). K.-K. N. acknowledges a NIST/NRC Postdoctoral Fellowship. We thank T. Fridley for his contributions and D. Gresh for discussions.

Supplementary Materials

www.sciencemag.org/content/342/6163/1220/suppl/DC1
Materials and Methods
Supplementary Text
Figs. S1 and S2
References (32–36)

24 July 2013; accepted 4 November 2013
10.1126/science.1243683